

RSC Advances



This is an *Accepted Manuscript*, which has been through the Royal Society of Chemistry peer review process and has been accepted for publication.

Accepted Manuscripts are published online shortly after acceptance, before technical editing, formatting and proof reading. Using this free service, authors can make their results available to the community, in citable form, before we publish the edited article. This *Accepted Manuscript* will be replaced by the edited, formatted and paginated article as soon as this is available.

You can find more information about *Accepted Manuscripts* in the [Information for Authors](#).

Please note that technical editing may introduce minor changes to the text and/or graphics, which may alter content. The journal's standard [Terms & Conditions](#) and the [Ethical guidelines](#) still apply. In no event shall the Royal Society of Chemistry be held responsible for any errors or omissions in this *Accepted Manuscript* or any consequences arising from the use of any information it contains.

Synthesis and NO_x Sensing Evaluation of Hollow/Porous La_{0.8}Sr_{0.2}MnO₃ Microspheres

Satoshi Suehiro, Hajime Okawa and Seiji Takahashi*

*Japan Fine Ceramics Center (JFCC), Material Research and Development Laboratory 2-4-1
Mutuno, Atsuta-ku, Nagoya 456-8587, Japan*

Email: s_suehiro@jfcc.or.jp

ABSTRACT

To improve nitric oxide (NO) gas reaction properties, we synthesized microspherical $\text{La}_{0.8}\text{Sr}_{0.2}\text{MnO}_3$ (LSM) particles. We investigated the NO sensing properties of NO_x sensors fabricated using electrodes based on hollow/porous LSM (*hp*-LSM) or solid sphere LSM particles. The *hp*-LSM particles were synthesized using a novel process combining spray pyrolysis with carbonization using citric acid. The resulting particles were characterized by X-ray diffraction (XRD), and scanning electron microscopy (SEM), and their specific surface area was estimated using Brunauer-Emmett-Teller (BET) theory. The particle and pore size of the *hp*-LSM particles were estimated to be 1-3 μm and 100-500 nm, respectively, and their highest specific surface area was determined to be 6.8 m^2/g . Sintered pellets made from *hp*-LSM particles had a relatively high density of 68 % and a broad pore size distribution between 100 and 1000 nm, estimated by the Archimedes method and mercury intrusion porosimetry measurements. The *hp*-LSM-based gas sensing electrode exhibited a faster NO response/recovery time than the one based on solid LSM. This synthetic method is expected to be widely applicable to other materials, and hollow/porous particles may be used for various applications such as gas sensors, batteries and chemical reactors.

INTRODUCTION

Perovskite-type oxide materials are very attractive for various applications such as in solar cells^{1,2}, electrodes^{3,4}, and catalysts^{5,6}. Lanthanum-based perovskite-type oxides of the composition $\text{La}_{0.8}\text{Sr}_{0.2}\text{BO}_3$ ($B = \text{Mn, Fe, Co, etc.}$) have mixed electronic-oxide ionic conductivity, and are used in the air electrode of fuel and metal-air batteries. Teraoka *et al.* have reported that the nitric oxide (NO) decomposition reaction in lanthanum-based perovskite oxides occurs through oxide ion vacancies⁷. For this reason, $\text{La}_{0.8}\text{Sr}_{0.2}\text{BO}_3$ has been extensively investigated for NO_x decomposition catalysis^{8,9} and for use in NO_x sensing electrodes^{10,11}. However, for those catalytic reactions, it is of vital importance that the gas diffusion and reaction area of $\text{La}_{0.8}\text{Sr}_{0.2}\text{BO}_3$ is improved.

Hollow spherical particles have been theorized to be superior electrode catalysts because of their relatively high specific surface area and low density. To date, such particles have been synthesized from metal oxides such as Co_3O_4 ¹², ZnO ¹³, TiO_2 ¹⁴, MnO_2 ¹⁵, and others, and been applied as catalysts¹⁶, in sensors¹⁷, and in batteries¹⁸. Often, spherical particles are obtained by spray pyrolysis using conventional template methods^{19,20,21}. Various template materials have been investigated, such as silica beads^{22,23}, polymers^{24,25} and carbon^{26,27}. However, template methods involve harsh chemical processes, are expensive, and suffer from low productivity. Therefore, there is a demand for new synthesis procedures that are industrially applicable. Additionally, few studies have evaluated the porosity of sintered hollow spherical particles.

Here, we report a novel process for the synthesis of hollow/spherical $\text{La}_{0.8}\text{Sr}_{0.2}\text{MnO}_3$

(*hp*-LSM) and solid spherical LSM (solid LSM) particles by combining spray pyrolysis with carbonization using citric acid. Furthermore, we evaluated the porosity of sintered *hp*-LSM and solid LSM particles. Finally, gas sensing electrodes were fabricated by deposition and calcination of LSM particles on yttria-stabilized zirconia (YSZ), and their amperometric gas sensing properties were studied.

EXPERIMENTAL

Chemicals

$\text{La}(\text{NO}_3)_3 \cdot 6\text{H}_2\text{O}$ (99.9 %), $\text{Mn}(\text{NO}_3)_2 \cdot 6\text{H}_2\text{O}$ (99.9 %) and citric acid (99.9 %) were purchased from Wako-Chemicals (Osaka, Japan). $\text{Sr}(\text{NO}_3)_2$ was purchased from Kanto Chemicals (Tokyo, Japan). Yttria-stabilized zirconia (8YSZ, 8 mol.% Yttria) was purchased from Japan Fine Ceramics (Miyagi, Japan). Pt paste (TR-7070) was purchased from Tanaka Kikinzoku Kogyo (Tokyo, Japan).

Synthesis of $\text{La}_{0.8}\text{Sr}_{0.2}\text{MnO}_3$ hollow/porous sphere particles

$\text{La}(\text{NO}_3)_3 \cdot 6\text{H}_2\text{O}$ (40 mmol), $\text{Sr}(\text{NO}_3)_2$ (10 mmol), $\text{Mn}(\text{NO}_3)_2 \cdot 6\text{H}_2\text{O}$ (50 mmol) and citric acid (500 mmol) were dissolved in water (500 mL). The resulting metal precursor solution was atomized using an ultrasonic wave generator, and the mist was reacted in a four-zone furnace at 200, 300 and 400 °C, and at 400 °C under N_2 flow (5 L/min). The produced precursor powders were carbonized by

decomposition of citric acid at 500-1000 °C for 1 h under N₂ flow (0.3 L/min). Finally, in order to remove carbon products, samples were heat-treated at 1000 °C for 2 h under air flow conditions (1 L/min).

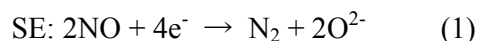
Materials Characterization

The synthesized crystals were analyzed by X-ray diffraction (XRD) using CuK α radiation (RINT2100, Rigaku, Tokyo, Japan), scanning electron microscopy (SEM) (JEM-2000EX/T, JEOL, and SU-8000, Hitachi, Tokyo, Japan), Brunauer-Emmett-Teller (BET) theory using a sorption analyzer (BELSORP-mini II, MicrotracBEL, Osaka, Japan), and mercury intrusion porosimetry (Auto Pore 9420, micromeritics, Norcross, GA, USA).

Sensor Fabrication and NO gas sensing Characterization

A practical amperometric sensor was fabricated as previously reported²⁸. LSM powder and ethylene glycol were mixed in a 2:1 weight ratio to prepare an LSM slurry, which was then screen-printed on one side of an 8YSZ pellet as the sensing electrode (SE). After LSM deposition, pellets were annealed at 1100 °C for 1 h. As the counter electrode (CE), Pt paste was screen-printed on the other side of the 8YSZ pellet ($\phi = 9$ mm, $t = 1$ mm), followed by annealing at 1200 °C for 1 h. This practical sensor was then attached to the tip of a magnesia tube, and the completed sensor was placed on the center part of a tubular electric furnace. The reaction curves for the sensor were

measured with a potentiostat (Solartron-1287, Solartron, Farnborough, UK), using an applied potential of -50 mV (*vs.* Pt-CE) at 450 °C. Complex impedance measurements were taken in the frequency range of 10^{-1} - 10^5 Hz, with an amplitude voltage of 10 mV. It was assumed that the electrochemical reaction on each electrode proceeds according to equations 1 and 2²⁸.



When a negative voltage is applied to the SE, NO is decomposed into N_2 and O^{2-} , and the O^{2-} is then moved to the CE by the potential gradient. The flowing current thus gives a sensor signal output in the external circuit. The NO sensitivity was estimated using the following formula:

$$\text{NO sensitivity} = \frac{I_{\text{NO}} - I_{\text{air}}}{I_{\text{NO}}} \times 100 (\%) \quad (3)$$

with I_{NO} the current measured in air containing NO and I_{air} the current measured in base air.

RESULTS AND DISCUSSION

Figure 1(a) shows the XRD patterns of the metal precursor powders after carbonization at temperatures of 750, 900, and 1000 °C. Samples at 750 °C exhibited a low crystallite content structure with a pattern assigned to MnO. With the higher carbonization temperatures of 900 and 1000 °C, on the other hand, we observed a pattern of high perovskite oxide and $\text{La}(\text{OH})_3$ crystallite content. Figure 1(b) shows the XRD pattern of samples carbonized at temperatures of 750, 900, and 1000 °C, after subsequent removal of the carbon through heat treatment. All sample spectra were in

good agreement with the LSM reference pattern (JCPDS No. 89-0648). The crystallite size of the 750, 900, and 1000 °C samples, estimated using the Scherrer equation, was estimated to be 13.3, 14.8 and 16.6 nm, respectively. Figure 2(a-c) shows the SEM images of synthesized metal precursor particles carbonized at 750, 900, and 1000 °C. Particles were spherical in shape, and the secondary particle size was *ca.* 1-3 μm. The particle shape and size were attributed to the mist size of sample solutions. Figure 2(d-f) shows the SEM images of LSM particles after carbon removal. At a carbonization temperature lower than 750 °C, the final LSM particles were solid spheres, whereas they contained voids when temperatures higher than 750 °C were used. To further evaluate the microstructure of these LSM particles, we examined their cross-section by focused ion beam (FIB)-SEM (Figure 3), which showed that LSM particles can have two types of internal structure: porous when the particle size was larger than *ca.* 1 μm, and hollow when the particle size was smaller. Furthermore, the specific surface area of synthesized LSM particles was estimated using the Brunauer-Emmett-Teller (BET) theory (table 1), and the highest surface area of 6.8 m²/g was measured for particles carbonized at 900 °C for 1 h. The lower estimated surface area of particles carbonized at 1000 °C suggests an increased density of the particles due to the progression of sintering at elevated temperatures.

Table 1. Specific surface area of La_{0.8}Sr_{0.2}MnO₃ (LSM) particles estimated using the Brunauer-Emmett-Teller theory.

Carbonization conditions	500 °C for 12 h	750 °C for 3 h	800 °C for 1 h	900 °C for 1 h	1000 °C for 1 h
Specific surface area (cm ² /g)	3.9	3.8	5.3	6.8	5.8

A schematic illustration of the proposed *hp*-LSM particle synthesis mechanism, based on the above results, is shown in Figure 4. In brief, LSM precursor spherical particles were synthesized by spray pyrolysis using a citric acid-containing metal precursor solution. When the obtained particles were carbonized at 750 °C, citric acid-derived carbon did not aggregate and grow. As a result, the carbon could likely be removed at 1000 °C in air, and the void filled up by LSM crystal growth. When particles were carbonized at a temperature higher than 750 °C, on the other hand, carbon attained a large grain size inside the particles, which led to a porous/hollow structure after carbon removal and LSM crystallization. We also tried to synthesize hollow/porous particles of various other Lanthanum-based perovskite-type oxides using the same procedure. The XRD patterns and SEM images of LaFeO₃ and LaCoO₃, shown in Figures S1 and S2, indicate that the reported process might be widely applicable for the synthesis of porous metal oxides.

To estimate the degree of porosity of sintered pellets of *hp*-LSM (carbonized at 900 °C) and solid LSM particles (carbonized at 750 °C), we performed density measurements using the Archimedes method, and measured the pore diameter distributions using mercury intrusion porosimetry. Table 2 shows the porosity results using Archimedes measurements for samples sintered at 1200 °C.

Table 2. Porosity and density of sintered pellets of *hp*-LSM and solid LSM, estimated by the Archimedes method.

Sample	open porosity	closed porosity	total porosity	relative density
<i>hp</i> -LSM	29.4 %	2.6 %	32 %	68 %
solid LSM	32.1 %	1.5 %	33.6 %	66.4 %

After sintering, a slight difference in open and closed porosity could be observed between *hp*-LSM and solid LSM samples, but there was no significant difference in total porosity. However, the pore diameter distributions revealed significant differences, as shown in Figure 5. Sintered solid LSM had a uniform distribution of small pores in the range of 200-300 nm. The pore size of sintered *hp*-LSM, on the other hand, was broadly distributed in the larger size range of 100-1000 nm.

We evaluated the NO sensing properties of amperometric sensors fabricated with either *hp*-LSM (carbonized at 900 °C) or solid LSM particles (carbonized at 750 °C) as their SE component. Figure 6(a, b) shows low and high magnification SEM images of the solid LSM SE surface morphology. The initial film consisted of 0.5-3 μm aggregated particles and showed cracks on the film surface, suggesting film shrinkage after electrode sintering. The surface morphology of the *hp*-LSM SE, on the other hand, indicated that a porous membrane had formed (Figure 6(c, d)), with an estimated pore size of 100-500 nm.

Figure 7(a) shows the comparison between the response currents and NO sensitivities for electrodes with either *hp*-LSM or solid LSM as their SE, when exposed to base air or air containing 500 ppm NO. Solid LSM-based electrodes exhibited greater response currents than *hp*-LSM-based ones. In order to understand these results, we studied the complex impedance measurements, shown in Figure 7(b). Semi-circles at lower frequencies were observed, which we interpreted as the resistance gas reaction²⁸. This result also suggests that the surface area of sintered *hp*-LSM was smaller than that of solid LSM; as a result, its response currents were low. However, the *hp*-LSM SE did exhibit greater NO sensitivity than the SE made from solid LSM. The mechanism leading to this improved NO sensitivity is currently under consideration. Finally, we estimated the response and recovery time of the sensors when exposure changed from base air to sample gas containing 500 ppm NO at 450 °C. As shown in Fig. S2, the response and recovery time was estimated at 10-30 s and 16-39 s for *hp*-LSM and solid LSM electrodes, respectively. The faster response and recovery times for *hp*-LSM electrodes might be due to their broad pore size distribution. Careful control of the particle size and pore size may be necessary to improve the catalytic gas reaction.

CONCLUSIONS

Hollow/porous $\text{La}_{0.8}\text{Sr}_{0.2}\text{MnO}_3$ (*hp*-LSM) particles were synthesized by a combination of spray pyrolysis with carbonization using citric acid. The *hp*-LSM particles and their pores were approximately 1-3 μm and 100-500 nm in size, respectively, with a highest measured specific

surface area of 6.8 m²/g when the carbonization step was done at 900 °C for 1 h. A nitric oxide (NO) sensing electrode was fabricated by screen-printed deposition of an *hp*-LSM slurry on Ytria-stabilized zirconia. Despite the baking procedure, a porous membrane electrode was formed. Compared to the response currents of electrodes prepared from solid sphere LSM particles, those of *hp*-LSM electrode were low due to *hp*-LSM's decreased specific surface area after sintering. However, the NO-sensing electrode made from *hp*-LSM particles did demonstrate a relatively shorter NO response/recovery time, which might be due to the broad pore size distribution in the sintered *hp*-LSM. In conclusion, hollow/porous particles may be effective for gas reaction applications, and the reported process for their synthesis can potentially be applied for other porous materials as well.

ACKNOWLEDGMENTS

This work was supported by Grant-in-Aid for Scientific Research (C) No.16K05878.

REFERENCES

1. J. Burschka, N. Pellet, S. J. Moon, R. Humphry-Baker, P. Gao, M. K. Nazeeruddin, M. Grätzel, *Nature*, 2013, **499**(7458), 316-319.
2. M. M. Lee, J. T. Teuscher, T. Miyasaka, N. Murakami, H. J. Snaith, *Science*, 2012, **338**(6107), 643-647.

3. Y.-H. Huang, R. I. Dass, Z. -L. King, J. B. Goodenough, *Science*, 2006, **312**(5771), 254-257.
4. Y. Takeda, R. Kanno, M. Noda, Y. Tomida, O. Yamamoto, *J. Electrochem. Soc.*, 1987, **134**(11), 2656-2661.
5. J. Suntivich, K. J. May, H.A. Gasteiger, J. B. Goodenough, Y. Shao-Horn, *Science*, 2011, **334**(6061), 1383-1388.
6. Y. Nishihata, J. Mizuki, T. Akao, H. Tanaka, M. Uenishi, M. Kimura, T. Okamoto, Hamada, N. *Nature*, 2002, **418**(6894), 164-167.
7. Y. Teraoka, T. Harada, S. Kagawa, *J. Chem. Soc., Faraday Trans.*, 1998, **94**, 1887-1891.
8. Y. Teraoka, K. Kanada, S. Kagawa, *Applied Catalysis B: Environmental*, 2001, **34**(1), 73-78.
9. V. G. Milt, C. A. Querini, E. E. Miró, M. A. Ulla, *Journal of Catalysis*, 2003, **220**(2) 424-432.
10. M. L. Grilli, E. Di Bartolomeo, E. Traversa, *J. Electrochem. Soc.*, 2001, **148**(9), H98-H102.
11. E. Di Bartolomeo, E. Traversa, M. Baroncini, V. Kotzeva, R.V. Kumar, *J. Eur. Ceram. Soc.*, **2000**, 20(16), 2691-2699.
12. X. Lai, J. Li, B. A. Korgel, Z. Dong, Z. Li, F. Su, J. Du, D. Wang, *Angew. Chem. Int. Ed. Engl.*, 2011, **50**(12), 2738-2741.
13. Z. Dong, X. Lai, J. E. Halpert, N. Yang, L. Yi, J. Zhai, D. Wang, Z. Tang, L. Jiang, *Adv. Mater.*, 2012, **24**(8), 1046-1049.
14. J. Yu, W. Liu, H. Yu, *Cryst. Growth Des.*, 2008, **8**(3), 930-934.

15. M. Xu, L. Kong, W. Zhou, H. Li, *J. Phys. Chem. C*, 2007, **111**(51), 19141-19147.
16. P. M. Arnal, M. Comotti, F. Schüth, *Angew. Chem. Int. Ed.*, 2006, **45**(48), 8224-8227.
17. X.-L. Li, T.-J. Lou, X.-M. Sun, Y.-D. Li, *Inorg. Chem.*, 2004, **43**(17), 5442-5449.
18. Y. Yao, M. T. McDowell, I. Ryu, H. Wu, N. Liu, L. Hu, W.D. Nix, Y. Cui, *Nano Lett.*, 2011, **11**(7), 2949-2954.
19. J. H. Bang, K. S. Suslick, *Adv. Mater.*, 2009, **21**(31), 3186-3190.
20. G. Jian, L. Liu, M. R. Zachariah, *Adv. Funct. Mater.*, 2013, **23**(10), 1341-1346.
21. J. H. Bang, R. J. Helmich, K. S. Suslick, *Adv. Mater.*, 2008, **20**(13), 2599-2603.
22. X. Xu, S. A. Asher, *J. Am. Chem. Soc.*, 2004, **126**(25), 7940-7945.
23. X.W. Lou, C. L. Yuan, L. A. Archer, *Small*, 2007, **3**(2), 261–265.
24. Y. Lu, J. McLellan, Y. Xia, *Langmuir*, 2004, **20**(8), 3464-3470.
25. Y. Ma, L. Qi, J. Ma, H. Cheng, W. Shen, *Langmuir*, 2003, **19**(21), 9079-9085.
26. Sun, X. and Li, Y. “Ga₂O₃ and GaN semiconductor hollow spheres.” *Angew. Chem. Int. Ed. Engl.* **2004**, **43**(29), 3827–3831.
27. Y. Zhu, T. Ikoma, N. Hanagata, S. Kaskel, *Small*, **2010**, **6**(3), 471–478.
28. T. Ueda, T. Nagano, H. Okawa, S. Takahashi, *Electrochem. Commun.*, **2009**, **11**(8), 1654-1656.

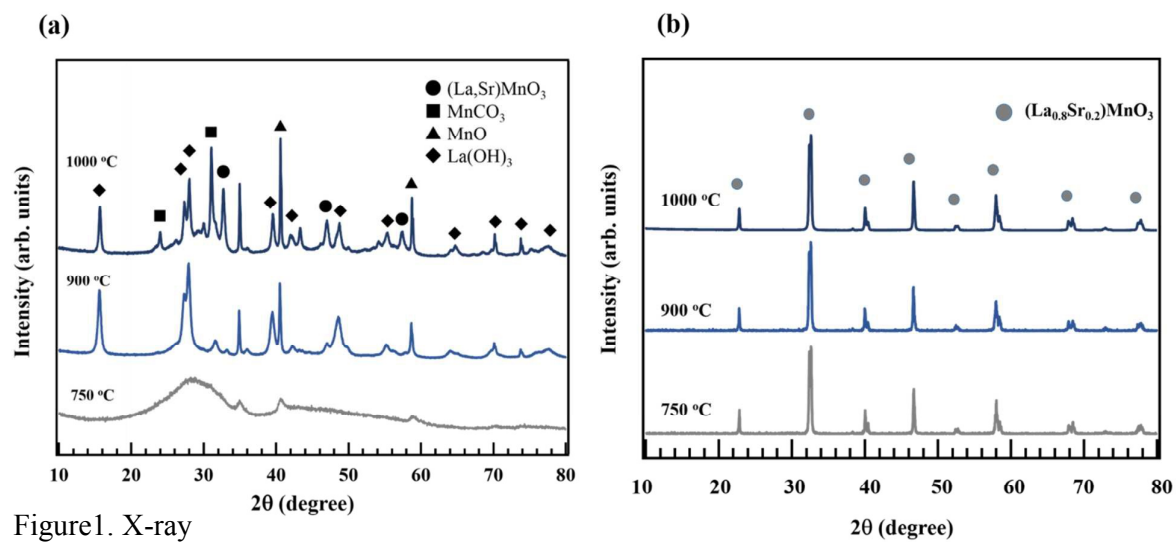


Figure 1. X-ray diffraction patterns of as-synthesized particles after carbonization at 750, 900 and 1000 °C (a), and the same carbonized particles after heat treatment at 1000 °C in air (b).

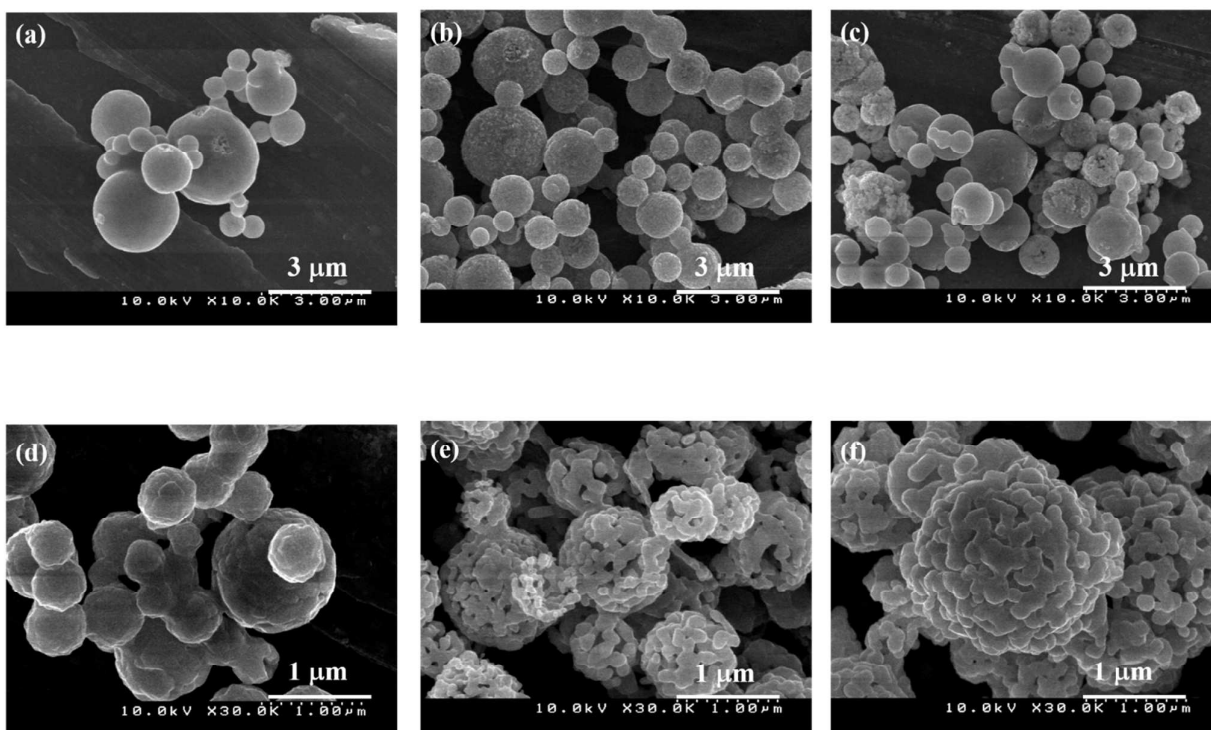


Figure 2. Scanning electron microscopy (SEM) images of as-synthesized particles after carbonization (a-c), and after subsequent heat treatment at 1000 °C in air (d-f). Particles were carbonized at 750 (a, d), 900 (b, e) and 1000 °C (c, f).

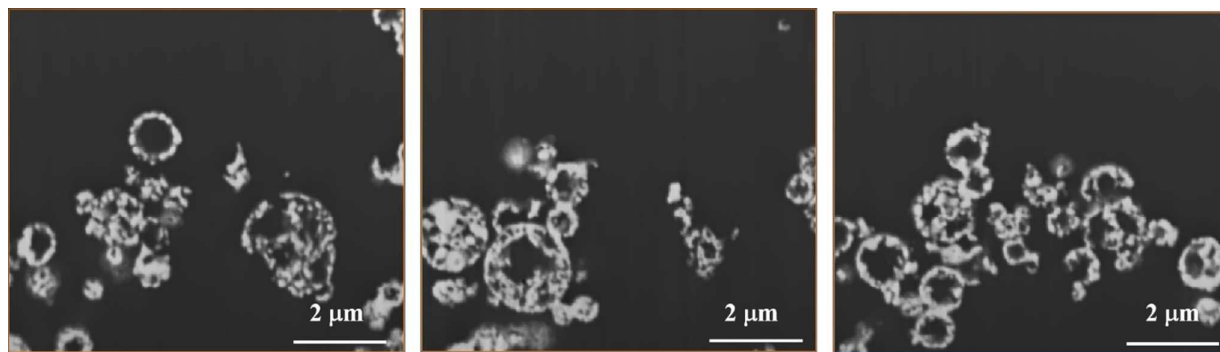


Figure 3. Focused ion beam (FIB)-SEM images of synthesized hollow/porous $\text{La}_{0.8}\text{Sr}_{0.2}\text{MnO}_3$ (*hp*-LSM) particles.

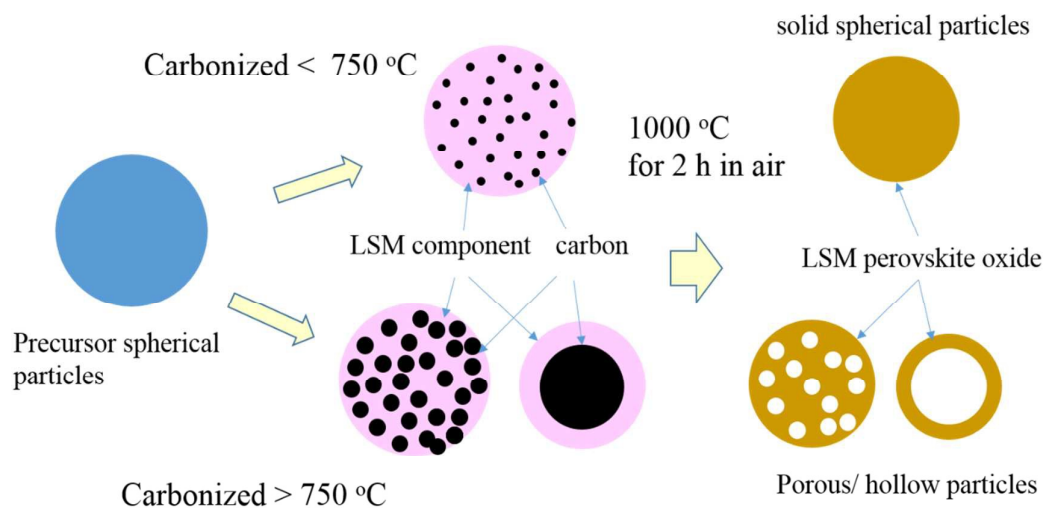


Figure 4. Schematic illustration of the possible mechanism of *hp*-LSM particle synthesis.

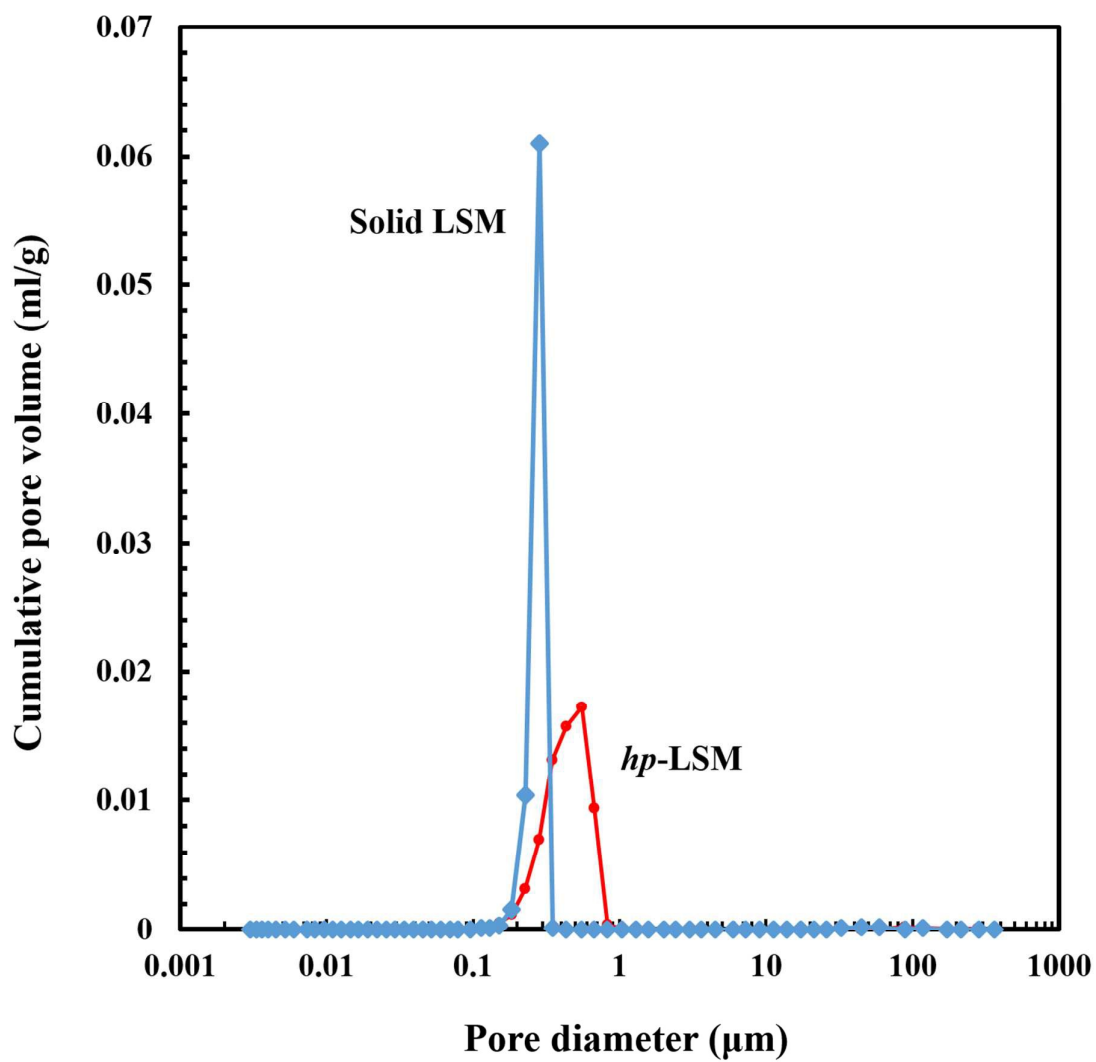


Figure 5. Pore size distributions of sintered pellets made from either *hp*-LSM or solid LSM, estimated by mercury intrusion porosimetry.

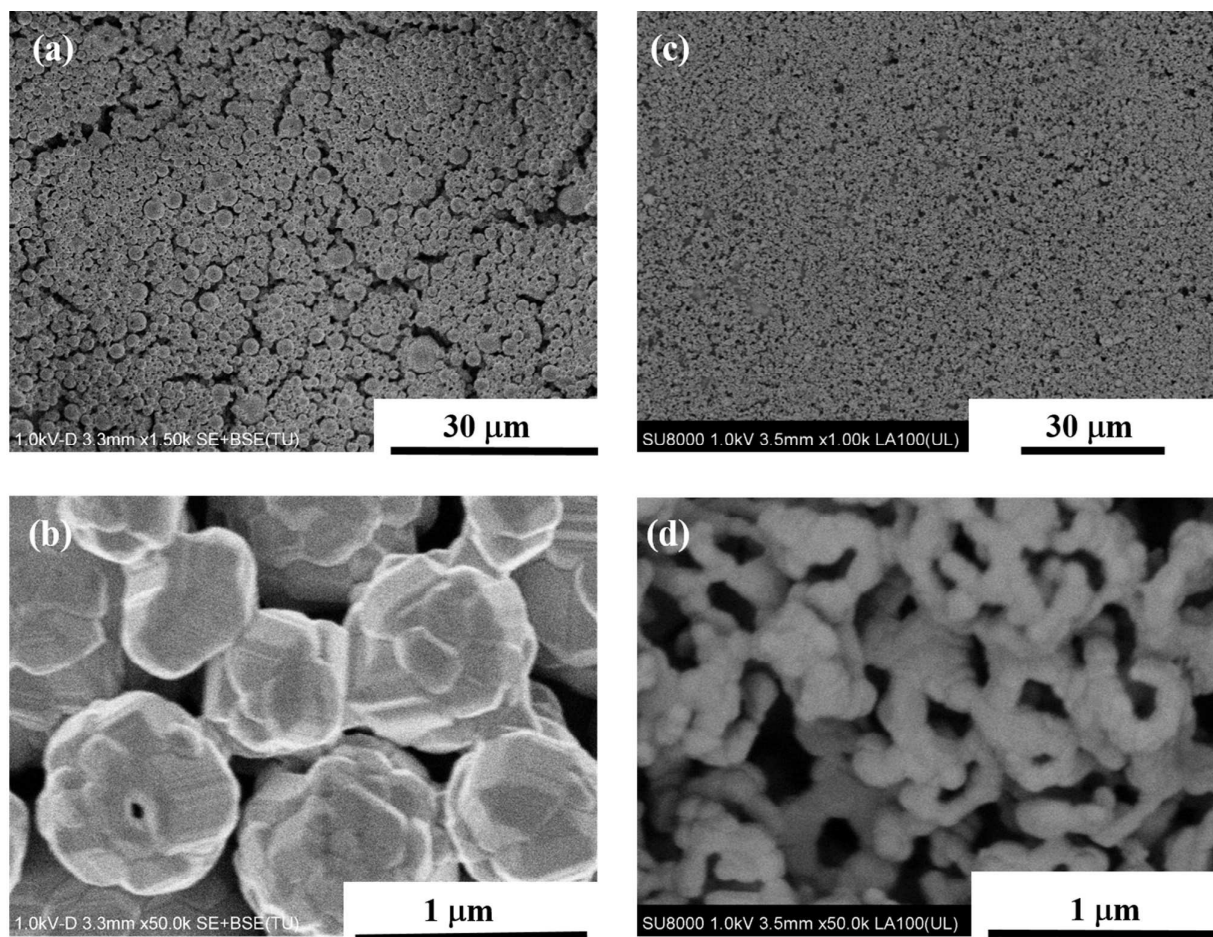


Figure 6. High and low magnification SEM images of the surface morphology of screen-printed $\text{La}_{0.8}\text{Sr}_{0.2}\text{MnO}_3$ (LSM) electrodes using either solid sphere LSM (a, b) or *hp*-LSM particles (c, d).

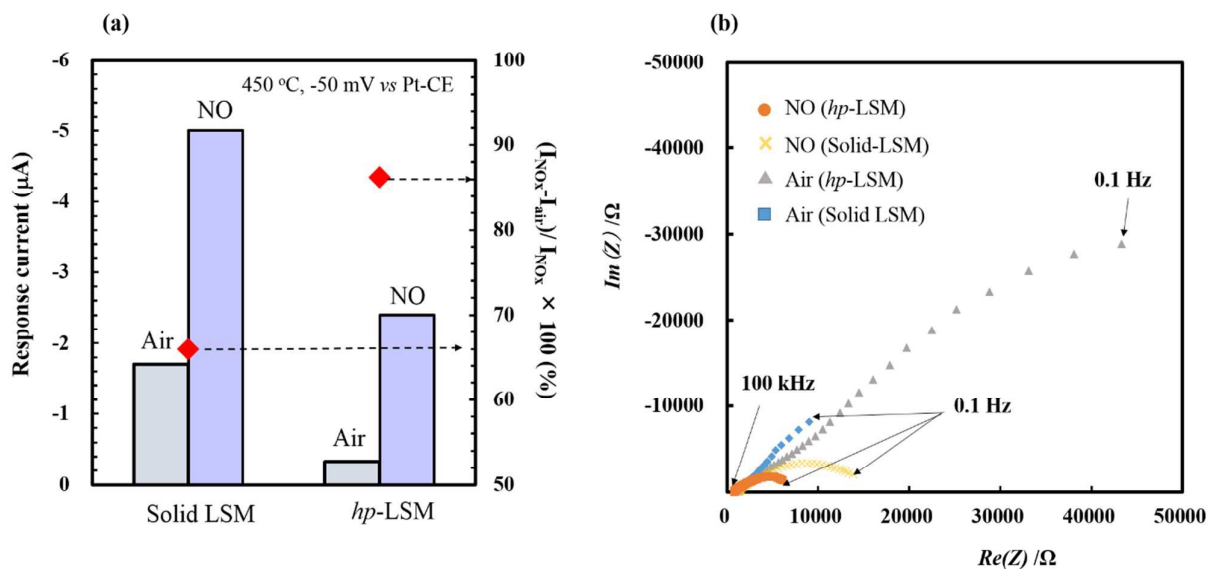


Figure 7. Response currents (bar graph) (a), NO sensitivity (◆) (a), and Nyquist plot (b) of sensors

fabricated using either solid LSM or *hp*-LSM, exposed to air or sample gas containing 500 ppm NO.

Table of contents entry

Fabrication $\text{La}_{0.8}\text{Sr}_{0.2}\text{MnO}_3$ electrode using hollow/ porous spherical particles and evaluated NO gas sensing response for NOx gas sensor.

